Chapter 5

Vegetated surface-scattering model for X and L bands with application to leaf area index and soil moisture retrieval and validation

5.1 Introduction

The development of a bistatic radar system or a concept of companion satellite to an existing sensor for Earth exploration is an emerging technique that can potentially enhance monostatic approaches. However, developing a bistatic radar system foresees several challenges such as sensors-technological challenges, cost challenges, environmental characterization challenges, and methodological challenges to develop a scattering model for different targets that allows consideration of experimental bistatic scattering response at ground and aircraft altitude [154].

Significant advancements have been made after the European Space Agency supported the concept of companion or multi-static satellites for different scientific objectives in the field of the cryosphere, biosphere, and solid Earth research [32]. The measurement of high precision data and exploiting bi/multi-static observation for monitoring land surface, vegetation, forest, ice, and ocean from active (i.e., synthetic aperture radar systems) and passive (i.e., radiometry) systems present sensors technological challenges for specific application requirements. The concept of companion satellite to existing sensors such as Sentinel-1, TerraSAR-X, Global Navigation Satellite System- Reflectometry (GNSS-R), and SAOCOM satellite is adopted to provide a cost-effective bi/multi-static geometry solution [32, 34–36]. The accurate quantification of different environmental parameters such as vegetation biophysical, land surface, snow water equivalents, tiny facets on the ocean surface, and atmospheric propagation conditions is necessary to understand the interaction characteristics of electromagnetic radiation with matter. Most of the initial demonstrations of bistatic observable quantities for land surface applications were measured using towers followed by aircraft, stratospheric balloons, and low Earth orbits through GNSS-R techniques [33]. The bistatic scattering echo from the vegetated rough soil surface is simultaneously affected by land and above-ground vegetation biophysical parameters. Therefore, the problem of monitoring and retrieving vegetation biophysical and land surface parameters using bistatic scattering responses is still challenging and interesting to solve.

In this Chapter, the primary objective is the instrumentation of the bistatic scatterometer system to test the capability of bistatic specular geometry for leaf area index (LAI) and volumetric soil moisture (m_v) monitoring using X and L bands scattering observations. The objective also includes the development of the microwave scattering model to simulate the time-series bistatic specular scattering coefficient (σ^0_{pq}) from vegetated (i.e., wheat crop) rough soil surface based on the coherent and incoherent scattering theory [85]

and its validation with the experimental observations. The approximations and iterative solution technique are used to solve the radiative transfer equation to find incoherent components of σ^0_{pq} for vegetated rough soil surface [3]. In the proposed scattering model, the vector formulation of Kirchhoff's approximation is used to model the rough soil surface scattering [85]. However, the complexities of modeling scattering phase matrix for canopy constituents are characterized by using parametric Henyey-Greenstein (HG) function [67, 151]. Further, a constraint non-linear least square estimation algorithm is used to optimize model parameters. Additionally, the model inversion evaluates the m_v and *LAI* retrieval.

5.2 Bi-spec scatterometer system and in-situ measurments description

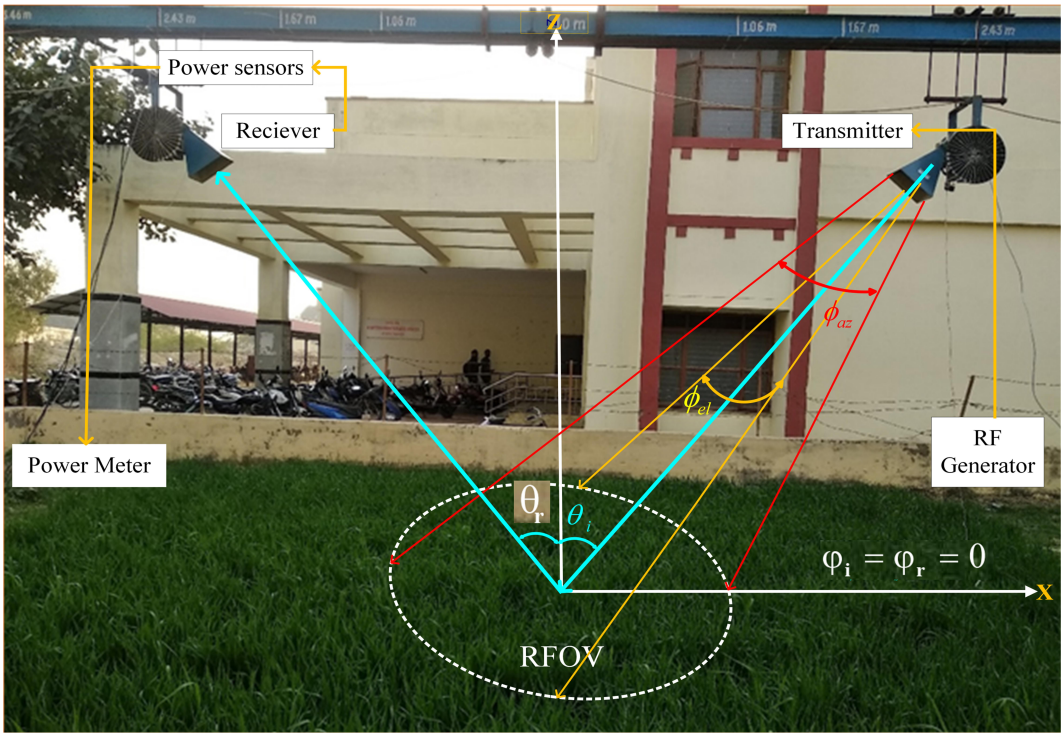

Fig. 5.1 The bistatic specular scatterometer system.

Two horn antennae (Pasternack make) bistatic scatterometer system was designed, as shown in Figure 5.1, to assess the capability of the bistatic radar system in a specular plane for soil moisture and leaf area index retrieval. The technical specifications of the bistatic scatterometer system are tabulated in Table 5.1. The transmitter and receiver antennas are connected to the rotator for zenith angle variation and mounted on the horizontal railing track at an altitude of $3m$. The experiments were performed on the specifically prepared wheat crop bed of area $10m \times 10m$ beside the Department of Physics, Varanasi, IIT(BHU). The bistatic scattering response measurements were started from January 14, 2020 (i.e., 20 days after sowing (DAS)) to March 20, 2020 (87 DAS). The scattering measurements were performed at five specular incidence angles from 20° to 60° at an interval of 10°. The bistatic scattering measurement from wheat crop and in-situ observations such as LAI and m_v were made on the same date for different phenological stages of the wheat crop. A total of eight scatterometer measurements were sampled between 20 to 87 DAS of the wheat crop. The scatterometer measurements were repeated four times on each day of the scatterometer sampling between 12 A.M to 4 P.M.. Further, the average value of four bistatic scattering responses was used to compute the final value of measured σ^0_{pq}. The polarimetric bistatic calibration technique that uses a large aluminum flat plate was used to calibrate vegetated rough soil surface scattering. The average of five measures within the sampling field was used as final LAI and m_v. The insitu LAI measurements were taken using the LAI-2200C plant canopy analyzer, and m_v observations were taken using Hydra Probe time-domain reflectometry sensor from a depth of $0-5cm$. The surface roughness profile was drawn on the $1m$ long soil profilometer with $1cm$ grid lines for the soil roughness parameter computation. Further, the surface roughness profiler image was digitized to compute the surface root mean square (RMS) height (s). In addition, the surface correlation length (l) was calculated using the Gaussian auto-correlation function.

Table 5.1 Specification of the bistatic scatterometer system

Parameters	Specifications	
Bands	X band	L band
Frequency used	10 GHz	2 GHz
Antenna Gain	20 dB	15 dB
Waveguide size	WR-90	WR-430
Beam-width V	16.5°	17.3°
Beam-width H	16.1°	17.4°
RF generator	High power continuous wave generator (PSG), (E8257D, 10 MHz–20 GHz)	
Power meter	The power meter of the EPM-P series (E4416A, 9 kHz to 110 GHz)	
Power sensor	Average and peak power sensor (E9327A, 50 MHz–18 GHz)	

5.3 Methodology

5.3.1 Problem formulation

The general framework of the bistatic scattering model is formulated using coherent and incoherent scattering components as shown in Equation 5.1.

$$\sigma^0_{pq} = \sigma^{coh}_{pq} + \sigma^{incoh}_{pq} \tag{5.1}$$

(1) **Coherent component** (σ^{coh}_{pq}): This component originates as a result of microwave transmission through vegetation, is attenuated, reflected by soil, and then attenuated again by retaining coherence in the specular direction. The average soil surface coherent field is implemented as the effective flat surface reflectivity multiplied by the gaussian RMS height distribution function [85]. Therefore, the coherent field scattered from the vegetated

rough soil surface in the forward specular direction ($\theta_r = \theta_i, \phi_i = \phi_r = 0$) is formulated as

$$\sigma_{pq}^{coh} = |R_{pq}(\theta_i)|^2 e^{-h^2 cos^2\theta_i} e^{-\frac{2\tau}{cos\theta_i}} \delta_{pq} \tag{5.2}$$

$$R_{HH}(\theta_i) = \frac{\cos\theta_i - \sqrt{\varepsilon' - \sin^2\theta_i}}{\cos\theta_i + \sqrt{\varepsilon' - \sin^2\theta_i}} \tag{5.3}$$

$$R_{VV}(\theta_i) = \frac{\varepsilon'\cos\theta_i - \sqrt{\varepsilon' - \sin^2\theta_i}}{\varepsilon'\cos\theta_i + \sqrt{\varepsilon' - \sin^2\theta_i}} \tag{5.4}$$

Where, $R_{pq}(\theta_i)$ is the co-polarized (i.e., HH and VV) Fresnels reflection coefficients and $h = 2ks$ is surface roughness parameter. ε' and k are a real part of soil dielectric constant and wave vector . The value of ε' is computed using the Dobson model [155], and the land surface parameter used for computation is detailed in Table 5.2 [156]. τ is defined as the vegetation's optical depth. The empirical relation between τ and LAI $(i.e., \tau = C_{pq} * LAI)$ was employed to connect the temporal dynamics σ_{pq}^0 with the vegetation biophysical parameter. Here, C_{pq} is the polarized microwave frequency-specific parameter.

Table 5.2 Land surface parameters

Sand (%)	Silt (%)	Clay (%)	Bulk density (Mgm^{-3})	Particle density (Mgm^{-3})
12.8	65.1	22.1	1.49	2.58

(2) Incoherent component (σ_{pq}^{incoh}): The iterative solution of the radiative transfer equation considers the canopy constituents as homogeneous anisotropic weakly scattering medium to ignore multiple scattering components contribution. The incoherent bistatic scattering coefficient (σ_{pq}^{incoh}) is formulated as[3]

$$\sigma_{pq}^{incoh} = e^{-\frac{2\tau}{cos\theta_i}} \sigma_{pq}^{soil} + \sigma_{pq}^{veg} \tag{5.5}$$

Where σ_{pq}^{soil} and σ_{pq}^{veg} are the bistatic scattered signal from rough soil surface and vegetation canopy. The computation of zero-order solution ignores the canopy constituents scat-

tering, except for two-way extinction $(i.e., e^{-\frac{2\tau}{cos\theta_i}})$ contribution from vegetation medium. The soil surface roughness parameters such as s and l are assumed temporally invariant. The contribution of σ_{pq}^{soil} in $\theta_r = \theta_i, \phi_i = \phi_r = 0$ direction is characterized by the Kirchhoff approximation as detailed in [85].

$$\sigma_{pq}^{soil} = \frac{|R_{pq}(\theta_i)|^2}{2m^2} \tag{5.6}$$

Where m represents surface RMS slope and is defined in terms of $s = 1.55cm$ and $l = 14.86cm$ (i.e., $m = \frac{\sqrt{2}s}{l}$). However, the original formulation of the generalized Henyey-Greenstein function is used to characterize the vegetation phase matrix P in the value of σ_{pq}^{veg}. Hence, the scattering contribution from vegetation constituents is expressed as

$$\sigma_{pq}^{veg} = 4\pi cos\theta_i(1 - e^{-\frac{2\tau}{cos\theta_i}})\frac{w}{2}P \tag{5.7}$$

$$P = \frac{1}{4\pi}\frac{1-v^2}{(1+v^2-2v\cos\Phi)^{1.5}} \tag{5.8}$$

$$\cos\Phi = a\cos\theta_i\cos\theta_r + b\sin\theta_i\sin\theta_r\cos(\phi_i - \phi_r) \tag{5.9}$$

Where w represents single-scattering albedo of the vegetation medium. The phase angle Φ in Equation 5.9 is generalized to mimic off-specular and anisotropic scattering from vegetation medium by modifying the original scattering generalization function definition [152]. The parameter a is used to control the angular dependencies of scattering amplitude in the forward specular direction. However, the parameter b is optimized to the value of σ_{pq}^{0} to model the anisotropic effect from the vegetation medium. The parameter v in Equation 5.8 allows the consideration of temporal changes in vegetation's structural and physical properties in the receiver's direction.

5.4 Results and discussion

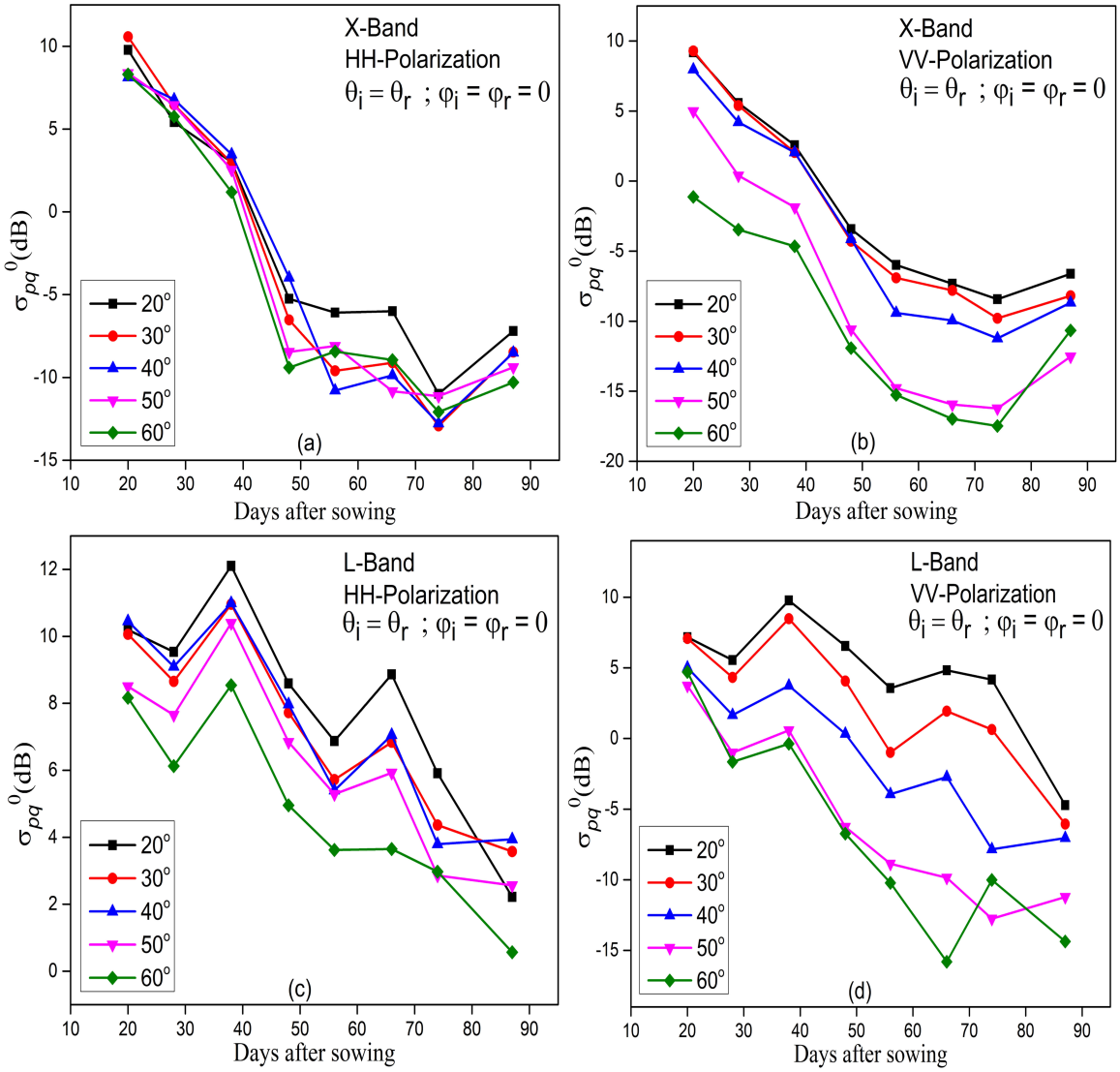

Fig. 5.2 Temporal variation in the measured σ^0_{pq} at HH and VV polarization for X and L bands.

The temporal variation of insitu measurements and computed ε' at different m_v values using the Dobson model for X and L bands are shown in Figures 5.3(a),(b). Figures 5.2(a)-(d) shows the multi-angular variation of the temporal curves of measured σ^0_{pq} at HH and VV polarization for X and L bands. The sensitivity analysis between the eight measured values of σ^0_{pq} and insitu observations (i.e., *LAI* and m_v) were performed based on

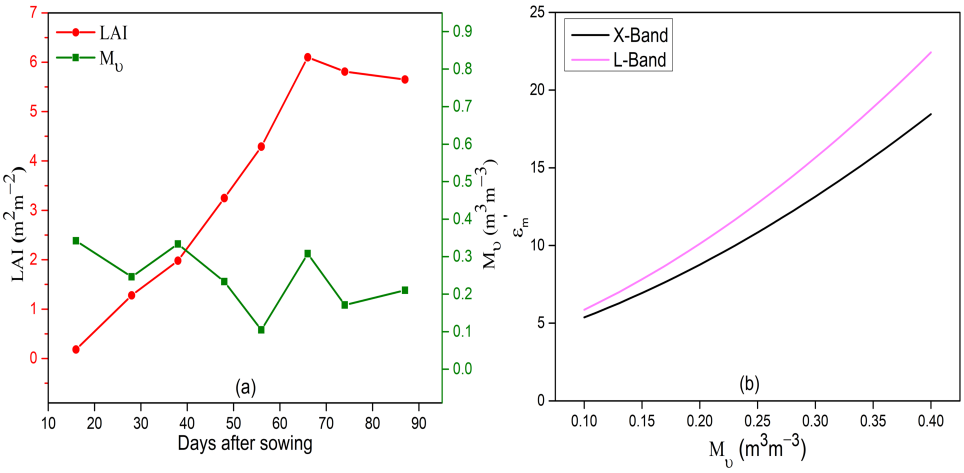

Fig. 5.3 (a) Temporal variation of insitu measurements; and (b) Computed ε' at different m_v values using the Dobson model for X and L bands.

the correlation analysis as shown in Table 5.3. An approximate decreasing trend (negative correlation) was reported between the measured σ^0_{pq} and *LAI* of the wheat crop for X and L bands. However, a positive trend (positive correlation) was found between the measured σ^0_{pq} and m_v. Specifically for the X band, the approximate decreasing trend was reported until the wheat crop's reproductive stage (i.e., 74 DAS). After the reproductive stage, vegetation biophysical parameters began to decrease due to defoliation of emerging leaves and inclination of the plant, leading to an increase in the measured σ^0_{pq}. For L band, the influence of m_v in the measured value of σ^0_{pq} is clearly visible in Figure 5.2(c), (d) due to its higher penetrating capability. However the influence of m_v in the measured σ^0_{pq} at lower specular incidence angle (i.e., 20° and 30°) and higher specular incidence angle (i.e., 60°) was found poor after the reproductive stage. It is due to the increase of vegetation scattering at lower incidence angle and higher effect of changes in the orientation of vegetation cover due to natural factors, like wind, at higher incidence angle. The correlation analysis between the measured σ^0_{pq} with *LAI* and m_v was found optimum at 40° at HH and VV polarization for X and L bands. Further, the optimum specular incidence angle of the bistatic scatterometer system is used to implement the microwave scattering model. For

computational simplicity, the optimum specular incidence angle is considered as 40° for L band VV polarization.

Table 5.3 Correlation analysis between 8 measured σ^0_{pq} with LAI and m_v

Incidence angle			20°	30°	40°	50°	60°
X band	HH	LAI	-0.940	-0.945	**-0.952**	-0.947	-0.926
		m_v	0.558	0.564	**0.589**	0.471	0.510
	VV	LAI	-0.965	-0.968	**-0.972**	-0.956	-0.916
		m_v	0.502	0.515	**0.551**	0.532	0.515
L band	HH	LAI	-0.690	-0.846	**-0.856**	-0.810	-0.846
		m_v	0.640	0.702	**0.737**	0.670	0.616
	VV	LAI	-0.601	-0.756	**-0.897**	-0.851	-0.864
		m_v	0.474	0.648	**0.654**	0.580	0.385

5.4.1 Model parameterization and optimization technique

The eight temporally measured values of σ^0_{pq}, insitu measurements (i.e., *LAI*, m_v and computed value of ε') between 20 DAS to 87 DAS were linearly interpolated to generate continuous data sets on a daily basis. Further, a total of 68 datasets daily are divided into calibration (70%) and validation (30%) data sets. The validation data sets were chosen systematically at an interval of 2-3 days to cover different phenological stages of the wheat crop. The calibration data sets were used to optimize the model parameters by minimizing cost function iteratively using a non-linear least square regression algorithm.

$$cost = min|\sum_{i=0}^{n}(meas\ \sigma^0_{pq_i} - sim\ \sigma^0_{pq_i}(b, C_{pq}, v, w))^2| \tag{5.10}$$

The model described in this letter mainly contains the parameterization of P, which is used to define the impact of vegetation cover scattering in the simulated value of σ^0_{pq} at various phenological stages of wheat crop. The model parameters are constrained such that the optimizing range of parameters is physically plausible based on the reference data sets. The weighting parameters a and b in Equation 5.9 mimic the anisotropic scattering

weightage due to the variation in the specular incidence angle and crop-specific anisotropy, respectively. The parameter a allows to approximate angular scattering dependencies in the simulated σ^0_{pq}. The numerical value of simulated σ^0_{pq} was found to increase with a and vice versa. The physically plausible numerical range of the parameter a was chosen between 0 <a< 1 to provide flexibility to the scattering model over a wide specular incidence angular range. For 40° optimum incidence angle (i.e., 40°), the numerical value of a was set at 0.5. The crop-specific anisotropic parameter (i.e., b) is optimized to the measured σ^0_{pq}. The parameter v plays an important role in simulating time series vegetation scattering from ideal forward specular scattering ($v = 1$; minimal/no vegetation) to forward isotropic scattering ($v = 0$; dense vegetation) for the bistatic geometry. The isotropic scattering increases with an increase in structural properties of the wheat crop. Therefore, the numerical value of v was optimized temporally at each phenological stage of the wheat crop based on measured σ^0_{pq}. For optimizing parameter v, a total of 20 data sets were generated based on the mean and standard deviation of four bistatic scatterings and five insitu measurements for each day of scattering measurement at different phenological stages of the wheat crop. Further, the linear interpolation of parameter v on daily basis is used to model temporal dynamics of direct vegetation scattering. The numerical values of the optimized model parameters in the forward modeling are shown in Table 5.4. The temporal variation in the optimized parameter v for X and L bands is shown in Figure 5.4. After model calibration, the optimized parameters are used to simulate temporal dynamics of σ^0_{pq}. The model performance for simulating σ^0_{pq} is tested against the validation data sets.

Table 5.4 Optimized model parameters at 40° specular incidence angle

Band	Polarization	Temporal range of v	b	C_{pq}	w
X	HH	0.626 > v > 0.345	1.958	0.458	0.036
	VV	0.612 > v > 0.355	1.971	0.431	0.047
L	HH	0.575 > v > 0.433	2.056	0.091	0.162
	VV	0.570 > v > 0.424	2.091	0.176	0.017

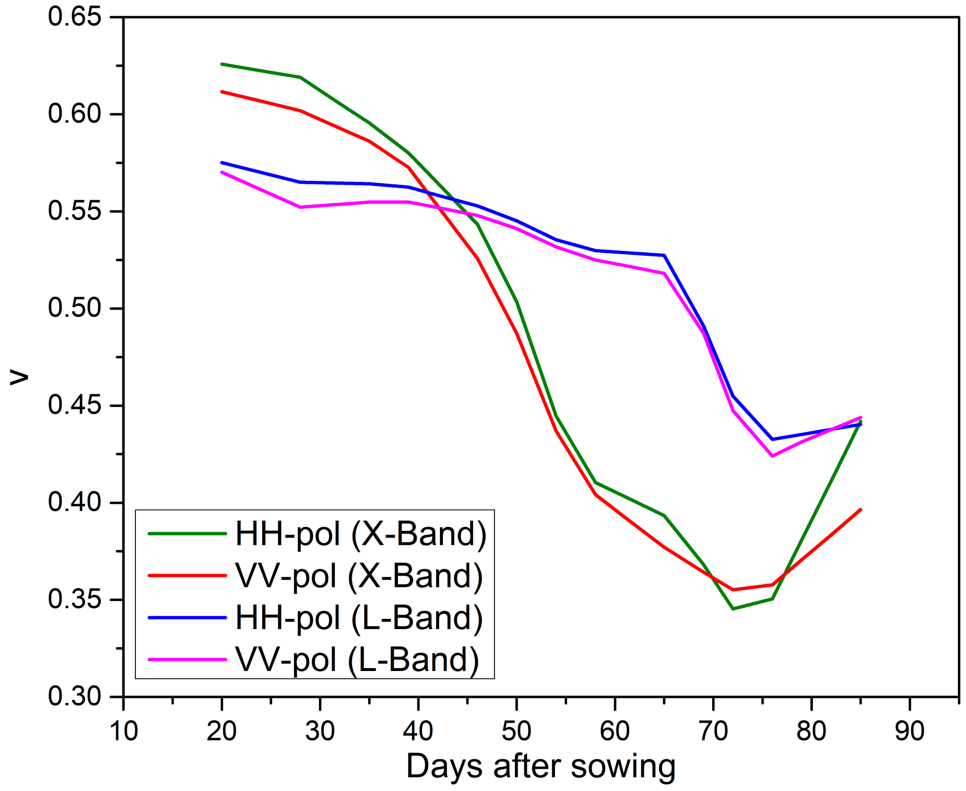

Fig. 5.4 Temporal variation of the optimized parameter v

5.4.2 Assessments of the bistatic scattering model results

The contribution of the coherent component and the two most significant incoherent components include attenuated direct soil (σ^0_{Asoil}) and direct vegetation (σ^0_{veg}) in the simulated σ^0_{pq} for X and L bands are shown in Figures 5.5(a)-(d). The coherent component is found significant for the L band, while its contribution is negligible for the X band. The effect of incoherent components in the simulated σ^0_{pq} offers an interpretation of time-series soil and vegetation scattering at different phenological stages of wheat crop. The incoherent vegetation component (σ^0_{Veg}) was found highly significant at HH and VV polarization for X band approximately after 40 DAS. In contrast, at HH polarization for the L band, the incoherent soil component attenuated by vegetation cover (σ^0_{Asoil}) was found dominant. However, the σ^0_{Veg} component shows dominance for the phenological stages of wheat crop between 45 to 70 DAS at VV polarization for the L band compared to

σ^0_{Asoil}. The possible reason is the higher loss of vertically polarized microwave signal with the vertically oriented lossy stalks of the vegetation and soil parameters due to its higher penetrating capability leads to the higher attenuation in the σ^0_{Asoil} component.

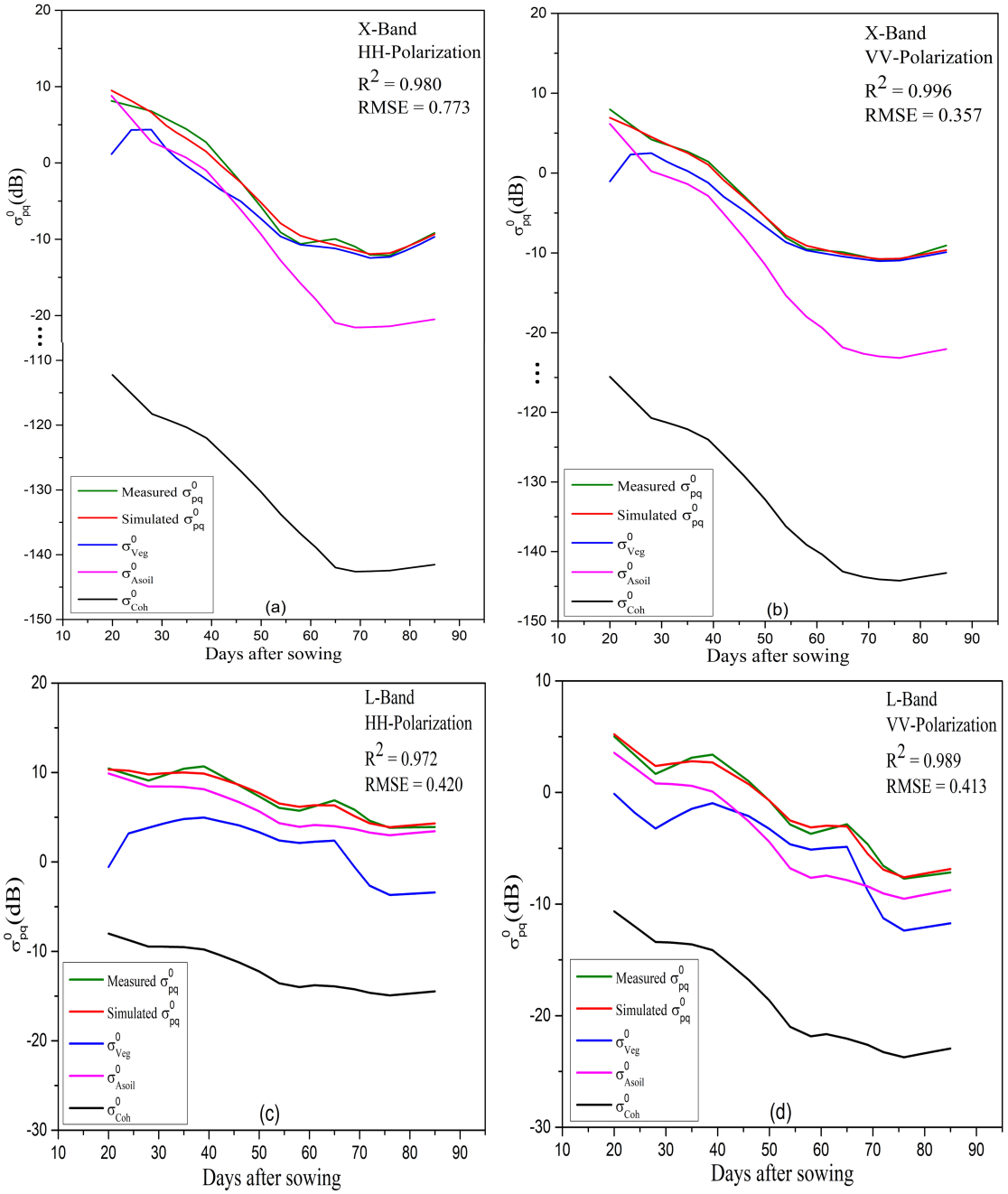

Fig. 5.5 The simulation results at HH and VV polarization for X and L bands.

5.4.3 Model inversion for LAI and m_v retrieval

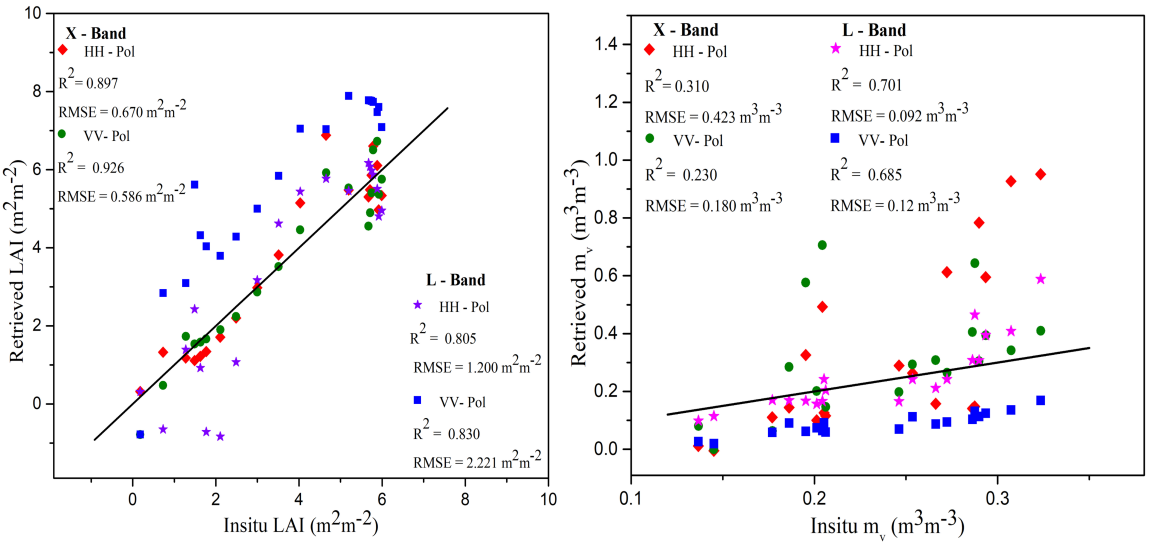

Fig. 5.6 *LAI* and m_v retrieval results

The LAI and m_v retrieval were performed from the calibrated microwave scattering model using an inverse non-linear least square algorithm on validation data sets. However, the retrieval process of m_v includes inversion of ε', which is forwarded to the Dobson model for m_v computation. The *LAI* and m_v retrieval accuracies were evaluated in terms of squared correlation coefficients (R^2) and root mean square error (*RMSE*) as shown in Figure 5.6. The performance of *LAI* retrieval at VV polarization for X band was found highly accurate with low RMSE $= 0.586 m^2 m^{-2}$ and high $R^2 = 0.926$. Whereas, the performance indices of m_v retrieval was found best with RMSE $= 0.092 m^3 m^{-3}$ and $R^2 = 0.701$ at HH polarization for L band.

5.5 Conclusion

In this Chapter, the idea of monitoring vegetation using the concept of bistatic geometry is exercised by designing a ground-based bistatic scatterometer system. The idea was developed to support the concept of a future bistatic/companion satellite mission for Earth

exploration. The experimental and developed bistatic microwave scattering model results in this study confirm the high potential of monitoring and retrieving land surface and vegetation biophysical parameters. The impact of the coherent component was found significant in simulated σ^0_{pq} for the L band compared to the X band. In addition, the inclusion of an approximate Kirchhoff's model in the incoherent scattering facilitates the approximation of soil surface scattering over different conditions of land surface parameters. The generalized Henyey-Greenstein function acts as a robust phase function to mimic incoherent vegetation scattering. The performance indices of *LAI* retrieval were accurate at VV polarization compared to HH polarization and m_v at HH polarization compared to VV polarization of X and L bands bistatic scatterometer data.

As a result, the proposed bistatic microwave scattering model could be viable for precise time-series monitoring and retrieval of vegetation biophysical and surface characteristics using the future Earth-Observing bistatic/companion satellite missions.

****